MEMS Single-Pole Double-Throw (SPDT) X and K-Band Switching Circuits

Sergio P. Pacheco, Dimitrios Peroulis and Linda P. B. Katehi

Radiation Laboratory
Department of Electrical Engineering and Computer Science
University of Michigan
Ann Arbor, Michigan 48109-2122 USA

Abstract— **Single-pole double-throw (SPDT) X and K-band circuit designs incorporating low-loss microelectromechanical shunt capacitive switches are reported. The switches incorporate highly inductive connecting beams which aid in further increasing the isolation at the desired operational RF frequency. Measurements show an isolation of better than 40 dB at both 7 and 20 GHz. Insertion loss was measured at -0.95 dB at 7 GHz and -0.69 dB at 20 GHz for the two respective designs.**

I. Introduction

Single-pole double-throw switch designs have traditionally evolved around solid state devices. These circuits usually are FET or PIN diode based and require considerable power to function, as well as the need for area consuming biasing and matching networks [1], [2], [3], [4].

Recently, there has been an astounding development of novel designs and applications of microelectromechanical systems (MEMS) in the microwave arena. This has been prompted mainly by the superior power consumption and intermodulation distortion characteristics of MEMS based devices over their solid state counterparts. MEMS devices have been successfully employed in applications such as high isolation switching [5], tunable capacitors [6], phase shifters [7], [8], [9], and filters [10].

In this paper, a compact shunt MEMS microwave switch [11] is used to replace solid state switches in a single-pole double-throw (SPDT) arrangement. The MEMS switch has the added advantage of being compact and not requiring matching networks. The SPDT designs presented here provide isolation and insertion loss in both the X-band (7 GHz) and K-band (20 GHz) frequency ranges that rival the performance of solid state switching circuits.

II. Resonant Switch

The switch used in this work was developed by Peroulis et al. for high isolation applications [10]. Their isolation characteristics depend on the on-state capacitance (C_{on}) presented by the center pad over the CPW center conductor when the switch is actuated and the parasitic inductance (L_s) introduced by the connecting beams as shown in the inset in Fig. 2. This series combination increases the isolation considerably around the resonant frequency given by

$$f_r = \frac{1}{2\pi\sqrt{C_{on}L_s}} \tag{1}$$

Therefore, careful consideration must be taken when selecting the connecting beam geometry so that the switch achieves resonance at the desired operational frequency. The values of L_s for three different connecting beam geometries were determined using the full wave electromagnetic solver IE3D[1]. Fig. 1 is a diagram of the connecting beams used in this study. The designs consist of a low inductive section represented by beam 1 and two high inductive sections (beams 2 and 3). The latter designs were specifically developed to resonate at X (beam 2) and K-band (beam 3) respectively. Table I lists the respective inductances and resonant frequencies for each of the connecting beam geometries from Fig. 1. First, it should be noted that in the X-band case, though the design frequency was 7 GHz, a higher resonant frequency

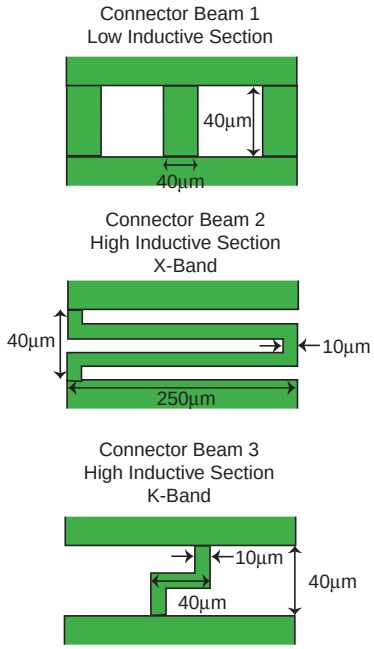

Fig. 1. Diagram of Connecting Beams for High Isolation (Also see Fig. 2)

[1] Zeland's IE3D, Release 6, 1999.

TABLE I
SIMULATED AND MEASURED INDUCTANCES AND RESONANT FREQUENCIES FOR CONNECTOR BEAMS IN FIG. 1

	Simulated		Measured	
	L_s	f_r	L_s	f_r
Beam 1 Low Ind.	1 pH	75 GHz	1 pH	75 GHz
Beam 2 High Ind. X-Band	63 pH	9.5 GHz	52 pH	10.4 GHz
Beam 3 High Ind. K-Band	14 pH	20 GHz	11 pH	22.6 GHz

(9.5 GHz) was used because the geometry needed for the connecting beams to achieve resonance at the operational frequency could not be easily realized in the gap between the center and actuation pads. Second, the measured high inductance values were approximately 20% lower than the predicted values by IE3D which caused a slight increase in the resonant frequency.

III. SPDT CIRCUIT DESIGN AND MODELING

A. Design

Fig. 2 shows a diagram of the SPDT switch design. The circuit consists of a tee with a MEMS switch at each of the output arms. The switch is placed at a distance of a quarter guided wavelength ($\lambda_g/4$) from the tee junction so that when the switch is actuated, the virtual RF short is translated to an open at the junction. Thus, the signal from the input port is reflected away from the arm containing the actuated switch and routed to the branch containing the other arm. The X and K-band circuits have MEMS switches located 1100 μm and 4350 μm away from the junction, which corresponds to $\lambda_g/4$ at 20 GHz and 7 GHz respectively. Thus, the RF responses for the two different circuits should present passbands centered around those frequencies. It should be also noted that the circuit response should actually repeat itself at odd multiples of the above frequencies due to the translation of the RF short into an open at odd multiples of $\lambda_g/4$.

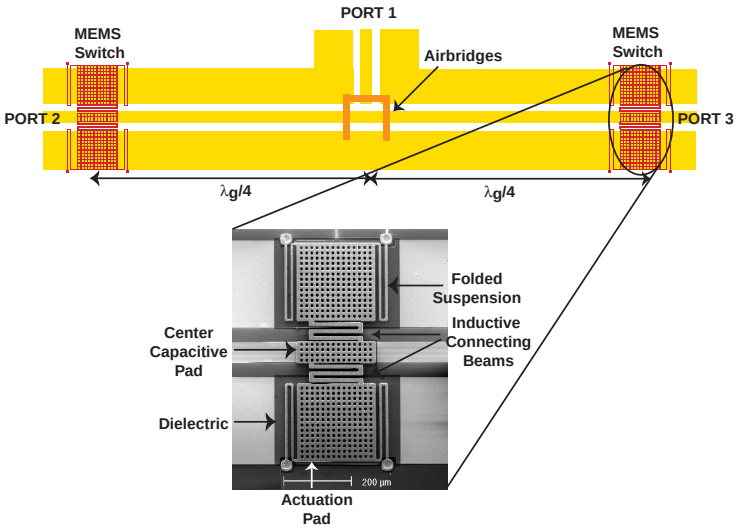

Fig. 2. Diagram of Single-Pole Double-Throw (SPDT) Circuit

X and K-band SPDT circuits containing one MEMS switch with the low inductive sections (beam 1) were fabricated and measured. In order to achieve the highest isolation at the desired operating frequencies of 7 and 20 GHz, the resonant high inductive X and K-band MEMS switches from Section II were placed at the appropriate distances at each arm of the SPDT circuit. In addition, a second high inductive resonant switch was placed at another $\lambda_g/4$ distance from the first one, thus further improving the isolation considerably. The circuits are 17.4 mm^2 and 4.4 mm^2 in area for the X and K-band designs, respectively.

B. Modeling

The circuits were modeled using HP EESof's Libra[2]. The model shown in Fig. 3 was developed for one single MEMS switch. The model consists of two sections of physical transmission line to represent the input and output sections of the FGCPW line and a capacitor-inductor-resistor series combination shunted across the transmission line to represent the MEMS switch. In this approach, the line impedance Z_0, line length l, and the effective dielectric constant ϵ_{eff}, are determined from the physical dimensions of the FGCPW line. The unloaded line attenuation, A, switch capacitances on, C_{on}, and off, C_{off}, inductance, L_s, and series resistance, R_s, are all varied to fit the model to the measured data. The attenuation in the physical transmission line model is specified at 20 GHz and then follows a $\sqrt{f}$ variation. Once the model parameters are determined for the single MEMS switch, the SPDT circuits are easily modeled by using the physical transmission lines to connect the switch section at the appropriate

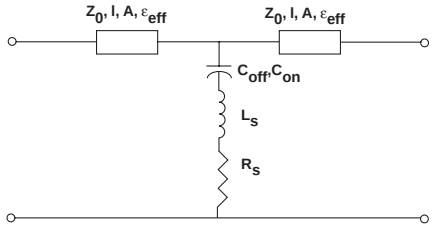

Fig. 3. Libra Lumped Element Model for Single MEMS Switch

[2]HP EESof Communications Design Suite v6.0, Hewlett-Packard Company, Santa Clara, CA, 1995.

distances away from the tee. Table II lists the physical parameters used to model the MEMS switch in this work.

TABLE II
PHYSICAL PARAMETERS FOR MODEL OF MEMS RF SWITCH

Z_0	50 Ω	C_{on}	3.5 pF
A	1.2 dB/cm	C_{off}	47 fF
ϵ_{eff}	6.3	L_s	1 - 52 pH
l	200 μm	R_s	0.3-0.8 Ω

IV. RESULTS AND DISCUSSION

The RF response of the system was measured using a 8510C Vector Network Analyzer, Alessi Probe Station, and GGB Picoprobe 150 μm pitch coplanar probes. A TRL calibration software, MULTICAL, developed at NIST [12], [13] is used to deembed the effects of the probe tips and feedlines from the measurement response.

The plot in Fig. 4 shows a comparison of the RF response of the X-band SPDT (a) insertion loss and (b) isolation between the low inductive (beam1) and high inductive (beam2) cases. Fig. 5 is a plot of the K-band SPDT (a) insertion loss and (b) isolation comparison for a low inductive (beam1) and high inductive (beam3) design. Note that in both cases there is very good agreement with the model presented in Section III. However, due to the noise floor limitations of the measurement system, it is not possible to attain an absolute value of the isolation for the K-band case (theory predicts approximately 90 dB). Nevertheless, in both X and K-band cases, there is a considerable increase in the isolation (almost twofold) as compared to the low inductive case. Also note that the switches resonate at a slightly higher frequency due to the deviation in inductance reported in Table I.

Table III summarizes the results of the tested circuits. It is important to note that the increase in isolation is accompanied by an increase in insertion loss across the passband. The loss due to individual MEMS RF switches is negligible [11]. The dominant force is the ohmic loss in the CPW lines and since in the high isolation cases the circuits are twice as long as in the low inductive designs, the loss increases accordingly. However, the insertion loss only degrades by at most 0.26 dB while the isolation achieves an improvement in performance of better than 20 dB in both X and K-band cases. These values are comparable and rival the performance of solid state SPDT switches.

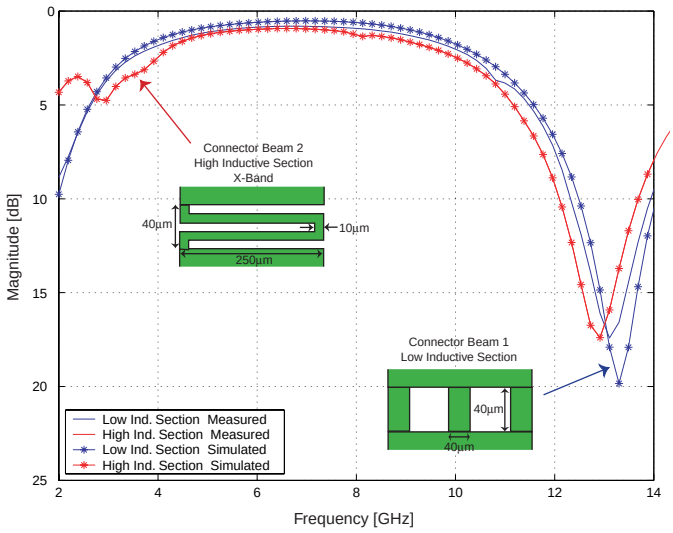

(a) Insertion Loss

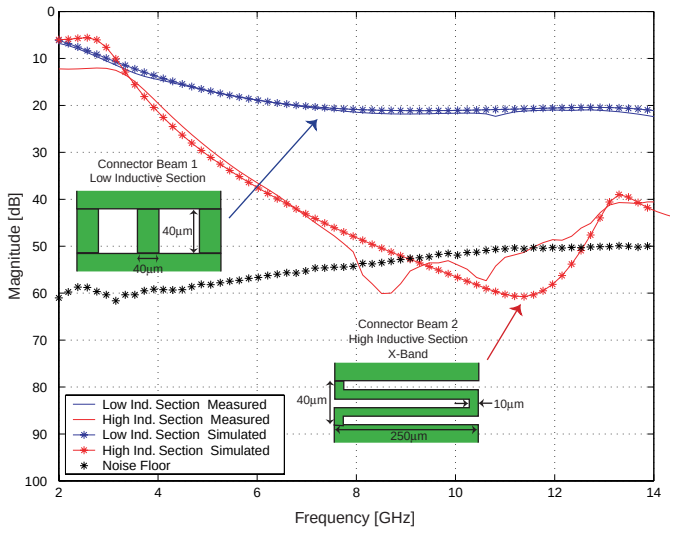

(b) Isolation

Fig. 4. Comparison of (a) Insertion Loss and (b) Isolation of X-Band Measured and Simulated Results for SPDT with Low and High Inductive Sections.

V. CONCLUSIONS

Through the use of compact and low-loss high isolation MEMS RF switches, SPDT circuits with excellent performance at X and K-band were demonstrated. The same treatment presented here can be extended to higher frequency ranges where the advantages of a higher on-state shunt capacitance and shorter arms would be very appealing for wireless applications. Furthermore, individually addressable switches on each arm of the SPDT configuration can conceivably be actuated in several different combinations in order to create frequency agile wide-band tuned switching circuits.

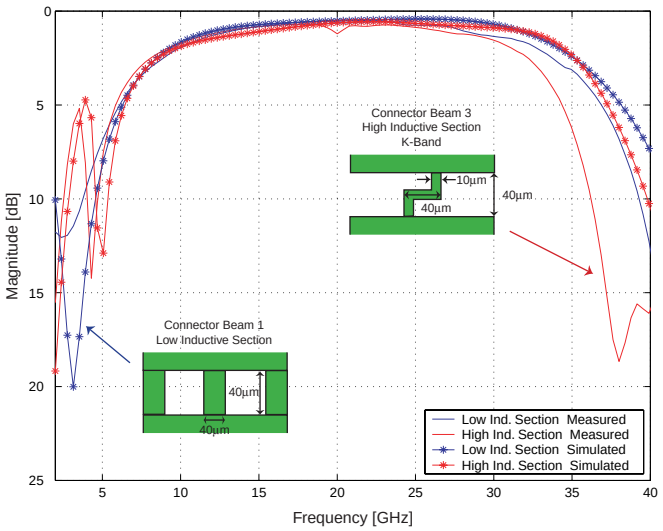

(a) Insertion Loss

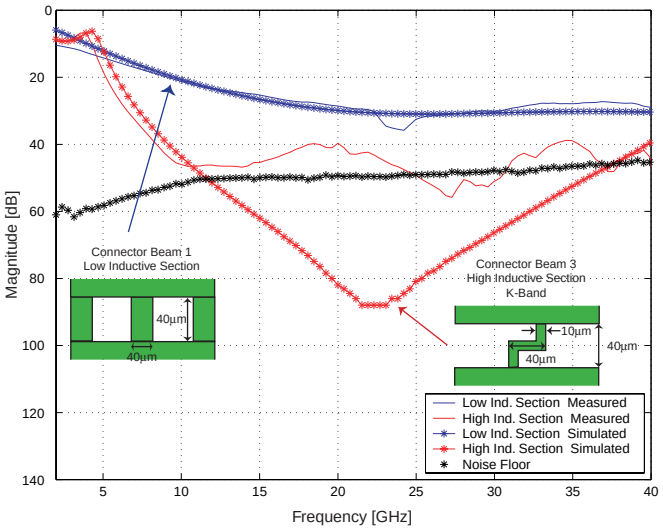

(b) Isolation

Fig. 5. Comparison of (a) Insertion Loss and (b) Isolation for K-Band Measured and Simulated Results for SPDT with Low and High Inductive Sections.

VI. Acknowledgments

The authors at the University of Michigan gratefully acknowledge the support of this research by the SOAC/JPL under the CISM Project, the Lockheed Martin Corporation under the RECAP Project, and the Department of Defense Research and Engineering (DDR&E) Multidisciplinary University Research Initiative (MURI) on "Low Power Electronics" managed by the Army Research Office (ARO) under Grant DAAH04–96–1–0001.

TABLE III
Measured Insertion Loss and Isolation Values for X-Band and K-Band SPDT Circuits

	X-Band	
	Low Ind. Switch	High Ind. Switch
Insertion Loss	-0.81 dB	-0.95 dB
Isolation	20.3 dB	43.3 dB
	K-Band	
	Low Ind. Switch	High Ind. Switch
Insertion Loss	-0.43 dB	-0.69 dB
Isolation	28.7 dB	50.0 dB†

† limited by the noise floor

References

[1] K. W. Kobayashi, L. Tran, A. K. Oki, and D. C. Streit, "A 50 mhz - 30 ghz broadband co-planar waveguide spdt pin diode switch with 45-db isolation," *IEEE Microwave and Guided Wave Letters*, vol. 5, pp. 56–58, February 1995.

[2] D. Teeter, R. Wohlert, B. Cole, G. Jackson, E. Tong, P. Saledas, M. Adlerstein, M. Schindler, and S. Shanfield, "Ka-band gaas hbt pin diode switches and phase shifters," in *IEEE MTT-S International Microwave Symposium Proceedings*, pp. 451–454, 1994.

[3] L. W. Ke, Y. J. Chan, and Y. C. Chiang, "Monolithic microwave algaas/ingaas doped-channel fet switches," *Microwave and Optical Technology Letters*, vol. 13, pp. 47–49, September 1996.

[4] H. Mizutani and Y. Takayma, "A dc-60 ghz gaas mmic switch using novel distributed fet," in *IEEE MTT-S International Microwave Symposium Proceedings*, pp. 439–442, 1997.

[5] J. B. Muldavin and G. M. Rebeiz, "30 ghz tuned mems switches," in *IEEE MTT-S International Microwave Symposium Proceedings*, pp. 1511–1514, 1999.

[6] Z. Feng, W. Zhang, B. Su, K. F. Harsh, K. C. Gupta, V. Bright, and Y. C. Lee, "Design and modeling of rf mems tunable capacitors using electro-thermal actuators," in *IEEE MTT-S International Microwave Symposium Proceedings*, pp. 1507–1510, 1999.

[7] N. S. Barker, *Distributed MEMS Transmission Lines*. PhD thesis, Univeristy of Michigan, 1999.

[8] J. S. Hayden and G. M. Rebeiz, "One and two-bit low loss cascadable mems distributed x-band phase shifters," in *IEEE MTT-S International Microwave Symposium Proceedings*, pp. 161–164, 2000.

[9] B. Pillans, S. Eshelman, A. Malczewski, J. Ehmke, and C. Goldsmith, "Ka-band rf mems phase shifters," *IEEE Microwave and Guided Wave Letters*, vol. 9, pp. 520–522, December 1999.

[10] D. Peroulis, S. Pacheco, K. Sarabandi, and L. P. B. Katehi, "Mems devices for high isolation switching and tunable filtering," in *IEEE MTT-S International Microwave Symposium Proceedings*, pp. 1217–1220, 2000.

[11] S. P. Pacheco, L. P. B. Katehi, and C. T.-C. Nguyen, "Design of low actuation voltage rf mems switches," in *IEEE MTT-S International Microwave Symposium Proceedings*, pp. 165–168, 2000.

[12] R. B. Marks and D. F. Williams, "Program multical," tech. rep., NIST, August 1995. Rev. 1.

[13] R. B. Marks, "A multiline method of network analyzer calibration," *IEEE Transactions on Microwave Theory and Techniques*, vol. 39, pp. 1205–1215, July 1991.